

---

# BVI-RLV: A Fully Registered Dataset and Benchmarks for Low-Light Video Enhancement

---

Ruirui Lin, Nantheera Anantrasirichai, Guoxi Huang,  
Joanne Lin, Qi Sun, Alexandra Malyugina, David R Bull  
Visual Information Laboratory, Bristol Vision Institute (BVI),  
University of Bristol, Bristol, UK BS1 5DD  
{r.lin, n.anantrasirichai, guoxi.huang,  
joanne.lin, lj21475, alex.malyugina, dave.bull}@bristol.ac.uk

## Abstract

Low-light videos often exhibit spatiotemporal incoherent noise, compromising visibility and performance in computer vision applications. One significant challenge in enhancing such content using deep learning is the scarcity of training data. This paper introduces a novel low-light video dataset, consisting of 40 scenes with various motion scenarios under two distinct low-lighting conditions, incorporating genuine noise and temporal artifacts. We provide fully registered ground truth data captured in normal light using a programmable motorized dolly and refine it via an image-based approach for pixel-wise frame alignment across different light levels. We provide benchmarks based on four different technologies: convolutional neural networks, transformers, diffusion models, and state space models (mamba). Our experimental results demonstrate the significance of fully registered video pairs for low-light video enhancement (LLVE) and the comprehensive evaluation shows that the models trained with our dataset outperform those trained with the existing datasets. Our dataset and links to benchmarks are publicly available at <https://doi.org/10.21227/mzny-8c77>.

## 1 Introduction

Capturing videos in low-light conditions is necessary for various applications, including natural history filmmaking, biology, zoology, robotics, surveillance, and security. However, low-light video footage is problematic due to the interactions between the aperture, shutter speed, and ISO parameters, which cause various types of distortions. This is due to the inverse correlation of increased photon noise with decreasing light intensity, where increased sensor gain amplifies noise. Secondary characteristics such as white balance and color effects are also affected and require correction. While these distortions reduce perceived visual quality, the associated artifacts pose significant challenges to machine learning tasks such as classification and detection.

The performance of low-light *image* enhancement algorithms has significantly improved in recent years, primarily through the application of deep learning methods. Such techniques, however, cannot be applied directly to low-light *video* content as their application on a frame-by-frame basis causes temporal inconsistencies. Optimization of these methods for motion video is limited by the need for large and diverse datasets with aligned ground truth information. Unfortunately, low-light video enhancement (LLVE) is an ill-posed problem, meaning that obtaining clean ground truth information with accurate brightness is challenging.

The availability of aligned and accurate ground-truth data for low-light video research is limited. Hence, researchers often use synthesized datasets, which may not replicate real distortions accurately. Some work has been done with self-supervised learning methods [4]. However, while these methods

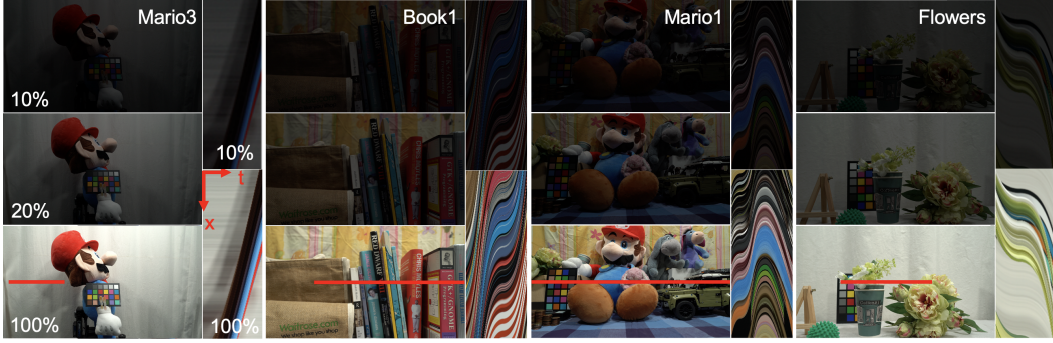


Figure 1: Scene examples with varying light levels and different motion profiles as shown in x-t plane. The length of the red lines across the normal-light frames represents the height of the x-t planes.

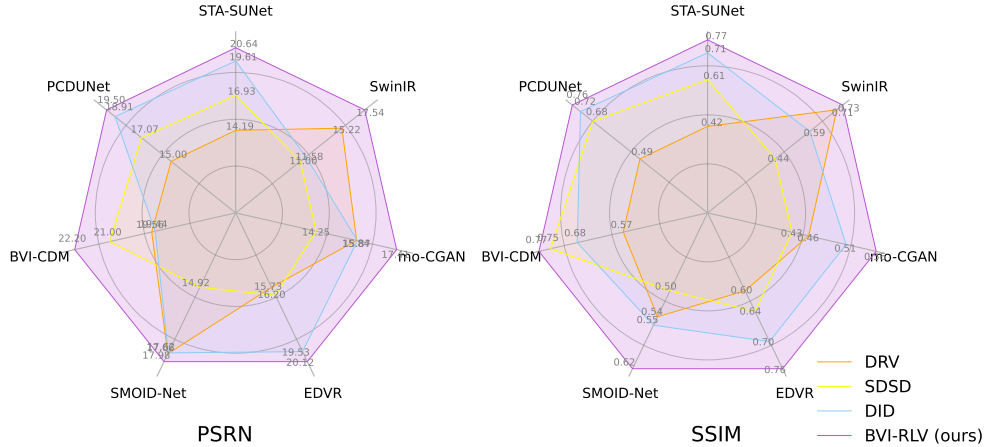


Figure 2: Models trained on BVI-RLV generate higher results compared to the other three LLVE datasets (i.e., DRV [1], SDSD [2], DID [3]). PSNR and SSIM are averaged across the four test sets. can achieve some level of contrast enhancement, they are not well-suited for color correction tasks. This is because low-light videos lack accurate color information, making color correction unfeasible, as confirmed by experiments in [5]. Alternatively, a pseudo reference with an unpaired learning strategy can be used [6], but these methods tend to be complex and require substantial memory.

To address these problems, this paper presents a dataset of fully registered sequences between real low-light videos and their ground truth, shown in Fig. 1, called BVI-RLV (Registered Low-light Videos). It was captured under three varying lighting conditions, with the 100% lighting condition classed as pseudo ground truth. The dynamic scenes were created using a programmable motorized dolly, allowing for repeatable motion profiles. Our dataset comprises a diverse range of forty scenes, containing various contents, structures, and textures, resulting in >30k ground-truth paired frames. Models trained with our BVI-RLV outperform those trained with other datasets, as shown in Fig. 2.

Due to the limited availability of quality datasets, there are not many low-light video enhancement methods to date. This paper hence provides four models for benchmarking. These models are based on different architectures: i) convolutional neural networks, PCDUNet, ii) transformers, STA-SUNet, iii) diffusion models, BVI-CDM, and iv) state space models, BVI-Mamba. We designed these four models to ensure that multiple GPUs are not required, allowing for wider usage in the community. We demonstrate the extensive and representative nature of our dataset in the context of supervised learning by employing it to train state-of-the-art models for image and video enhancement. Our experimental results show the significance of fully registered video pairs in the development of low-light video enhancement methods and comprehensive evaluation.

## 2 Related work

**Existing low-light datasets.** Several ‘image’-based datasets exist that can be used to support denoising and other inverse problems. These include the UCID-v2 corpus [12], the Darmstadt Noise Dataset [13], the Smartphone Image Denoising Database (SIDD) [14]. There are a couple of low-light

Table 1: Low-light video dataset comparison. S and D indicate static and dynamic scenes, respectively. 1D means one type of movement. D\* means stop motion.

Name	Light	Motion	Frames	Resolution	GT	Register	Release
BVI-LOWLIGHT [7]	Real	S	13,200	4240×2832	✓	✓	✓
DUS (Static) [8]	Real	S	3,630	2160×1280	✓	✓	✓
DUS (Dynamic) [8]	Real	D	15,000	2160×1280	✗	✗	✓
DRV (Static) [1]	Real	S	20,847	5496×3672	✓	✓	✓
DRV (Dynamic) [1]	Real	D	2,397	5496×3672	✗	✗	✓
BBD-100K [9]	Real	D	-	1280×720	✗	✗	✓
SMOID [10]	ND filter	1D	35,800	1800×1000	✓	✓	✗
RViDeNet [11]	Real	D*	385	1920×1080	✓	✓	✓
SDSD [2]	ND filter	1D	37,500	1920×1080	✓	Mix	✓
DID [3]	ND filter	1D	41,038	2560×1440	✓	✓	✓
<b>BVI-RLV (Ours)</b>	Real	D	31,800	1920×1080	✓	✓	✓

video datasets captured in static scenes, allowing for the creation of ground truth. This includes our BVI-LOWLIGHT, which offers true ISO noise in videos captured at 30 frames per scene [7], and DRV (also referred to as SMID) [1], capturing 60-100 frames per scene. The DRV also provides dynamic videos without ground truth, similar to the BBD-100K dataset [9]. The Dancing-under-the-stars dataset (DUS) [8] provides 26 static scenes, each with one clean image paired with noisy bursts, and 42 unpaired raw noisy dynamic videos for testing. The raw videos were captured with a high-end Canon LI3030SAI sensor. Table 1 shows the existing low-light datasets. Notably, only four datasets to date feature motion and provide ground truth (paired dynamic videos):

1. **SMOID** [10] consists of 179 pairs of street view videos, each with 200 frames in a GBRB Bayer pattern, captured simultaneously using a beam splitter and an ND filter. Only the overlapping area was used. Unfortunately, this dataset is not publicly available.
2. **RViDeNet** [11] was captured at five ISO levels from 1600 to 25600. Each video contains seven frames in Bayer format, captured using stop motion, resulting in no motion blur and large displacements between frames, causing unsmooth and unnatural motion. The clean frame, obtained by averaging multiple noisy frames, remains dark. Therefore, this dataset is unsuitable for brightness enhancement and color correction in low-light video enhancement.
3. **SDSD** [2] has 150 video pairs captured using a motorized dolly, but some frames are misaligned, making them unsuitable for supervised learning or objective evaluation. Our experiments confirmed this issue. Despite claims of using an ND filter and adjusted ISO settings, we found inconsistencies in lighting and shadows, and several reference videos are overexposed, obscuring details [3].
4. **DID** [3] has 413 video pairs, captured using five different cameras. Dynamic scenes were created with an electric gimbal, resulting in only one type of motion: panning. Video brightness was adjusted with an ND filter. We found some pairs are misaligned, and some videos have dirt on the lens.

These datasets are limited for developing reliable video enhancement tools due to their small size, lack of realistic distortions, or absence of ground truths for moving objects, affecting their suitability for training and validating new networks. Additionally, most datasets with ground truth use ND filters, which can cause color shifts, optical aberrations, reduced sharpness, reflections, lens flare, and degradation over time, impacting image quality and reliability.

**Existing methods for low-light video enhancement.** With recent advances in deep learning technologies, ‘*image*’ enhancement has made significant progress. In contrast, learning-based video enhancement techniques are still in their early stages [15], primarily due to more unknown parameters, limitations in datasets, computational complexity, and high memory requirements. Multiple input frames are typically used. SMOID [10] modified UNet [16] to handle multiple frames, but this method may not effectively handle fast motion. Therefore, several methods align the feature maps of neighboring frames with those of the current frame [2, 17]. Earlier work exploited recurrent neural networks [18], while later, Deformable Convolution Networks (DCN) [19] became more commonly employed for this purpose. An iterative process for re-weighting features is used to further minimize merging errors [17]. Liu et al. [20] proposed using synthetic events from video to adaptively combine multiple frames according to the speeds of moving objects. Fu et al. [3], who created the DID dataset, also proposed a light-adjustable network based on Retinex theory. Unfortunately, their code is not



Figure 3: (Left) Scene setting showing the camera in ‘angle’ position, mounted on CineDrive system. (Right) Moving bunny scene with static background showing pixel value difference between the normal-light frame and the adjusted low-light frame before and after alignment (gray = zero error).

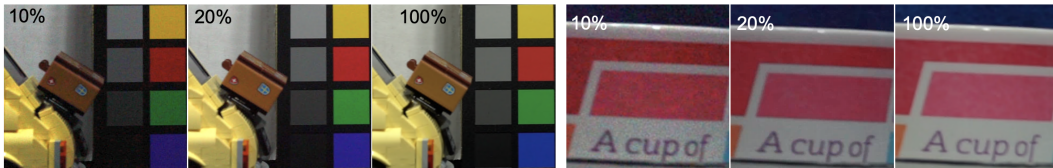


Figure 4: Cropped images (Lego and Kitchen scenes at  $350 \times 350$  and  $140 \times 140$  pixels, respectively) with histogram matching to the reference (normal light) to visualize noise at different levels of light.

publicly available. SDS-Net [2] separates noise and illumination to generate the output. Some methods require Bayer raw video inputs, which are unsuitable for consumer cameras [1, 10, 21].

### 3 Proposed low-light video dataset

**Controlled environment.** Acquisition of the new dataset was conducted in a dedicated studio, designed to permit full and precise control of the environment’s light intensities. Four Cineo MavX lights, with up to 8,000 lumens output, were used. The color temperature was set to 6,500 Kelvin. Our dataset of video pairs was recorded with low light at 10% and 20% of normal lighting levels (100%), as indicated by the Zero 88 FLX S24 light controller.

**Camera settings.** We used a consumer camera to maximize accessibility and usage applications to capture our video dataset. The consumer cameras provide the videos in RGB format. For raw format, only *some* high-end professional cameras provide that. This should not be confused with the ‘*image*’ raw format, which most consumer cameras allow users to access. If the reader would like to analyze noise and *image* processing pipeline, we refer to our low-light image dataset, BVI-LOWLIGHT [7], which use the same camera, a Sony Alpha 7SII with FE 16-35mm F2.8 GM lens.

We are aware that high-quality data is significant for low-level vision tasks. We captured our videos with minimal image signal processing (ISP) with the lowest compression – XAVC S format, the highest level supported by H.264, with 8-bit depth and full HD resolution ( $1920 \times 1080$  pixels). The ISO was fixed at 160 for normal light and at 800 for low light, the optimal value recommended by the manufacturer. The higher ISO will enable in-camera denoising. The white balance is set to match the light source (C.Temp./Filter mode). The frame rate was set to 25 fps, which led to a fixed shutter speed of  $1/50$ , as recommended by professionals to achieve a shutter angle of 180 degrees (equivalent to double the frame rate). The aperture was set at F6.3, which fell within the middle range of the camera’s optimal aperture setting, producing the most stable and highest image quality while ensuring consistent exposure. The focal length was adjusted to get the best composition for each scene and to ensure diverse scene variations. We used Sony’s Imaging Edge mobile app for camera triggering via Wi-Fi, avoiding unwanted shadows and sensor misalignments from manual triggering.

**Programmable motion control.** The repeat movement was controlled using a Kessler CineDrive shuttle dolly system. The CineDrive system, mounted on the dolly allowed additional horizontal camera movement and rotation in three axes (see Fig. 3 left). To ensure that the objects were visible throughout the entire length of the clipped videos, we manually selected the start and stop points.

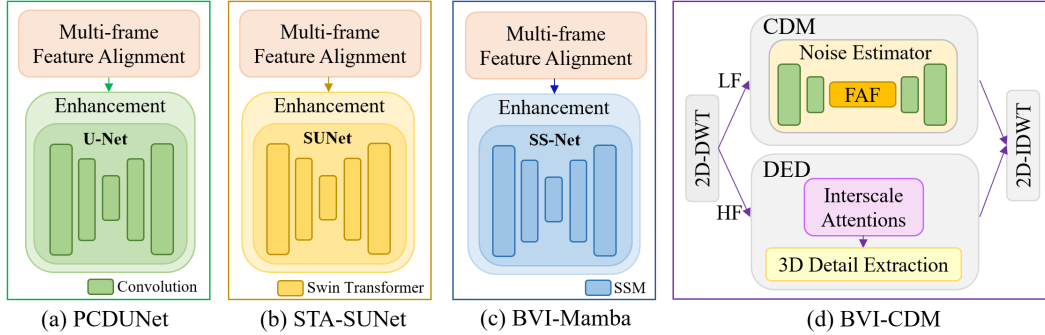


Figure 5: Main architectural components of the four different benchmarking methods, i.e., PCDUNet, STA-SUNet, BVI-Mamba and BVI-CDM.

### 3.1 Ground truth generation

The primary sources of misalignment are related to the mechanical tolerances of the shuttle dolly and the acceleration of the control motor. Despite careful setup of the mechanical system, there is a possibility of frame misalignment between any two identical motion profiles. The degree of misalignment also depends on the speed of motion. During testing of our CineDrive system, the maximum observed misalignment is 20 pixels. Given that the frame resolution is  $1,920 \times 1,080$  pixels, this is only 1% of the frame width.

We kept the low-light videos as they were because adjusting them could alter the noise characteristics and motion blur. Therefore, we generated pseudo ground truth registered to each frame of the low-light videos. ***Our approach is based on the principle that a very close pseudo reference is appropriate for training in many cases*** (as achieving good results shown in Section 5). We refrained from using warping techniques or non-rigid registration because our tests using them [22] created altered low-level features and sometimes introduced artifacts.

**Repetition strategy.** The ground truth videos were recorded under normal lighting. To minimize misalignment with the low-light videos, we repeated the dolly movement, creating three normal-light videos for slow motion and five for fast motion. This introduced slight pixel shifts, ensuring the best match to the low-light video had minimal misalignment. In most cases, the best matching video remained consistent throughout the video. However, in a few pairs, the best match changed due to a change in the dolly’s direction, such as moving left to right and then back to the left.

**Alignment procedure.** Firstly we cropped the video by 100 pixels from the borders of the frame to avoid the influence of the background. We subsequently enhanced the frame  $t$  of the low-light video  $J$  by matching its histogram of each color channel to the histogram derived from the normal-light frame  $I_n^m$  of the video  $m$  at frame  $n$ , i.e.  $\hat{J}_t = \mathcal{H}(J_t, I_n^m)$ , where  $\mathcal{H}$  is a histogram matching function [23] with 255 bins for images with an 8-bit depth. This can be seen as contrast enhancement and color correction with respect to the information from the reference (normal light in our case). Then, the best-aligned reference frame (normal light level) was found by minimizing the mean absolute error between  $\hat{J}_t$  and  $I_n^m$ , where  $n \in [t - N_w, t + N_w]$ ,  $N_w$  is a predefined searching window range,  $m \in [1, N_v]$ , and  $N_v$  is the total number of videos repeatedly captured at the same normal-light scene. Fig. 3 (right) shows error maps depicting the differences between the low-light frame and the normal-light frame before and after frame alignment.

**Alignment accuracy.** We verified the accuracy of our alignment technique using two approaches. First, we calculated the pixel shift across all the scenes using Normalized Cross-Correlation [24] and found an average alignment error of 0.256 pixels with a standard deviation of 0.451 pixels. Secondly, we detected the corners in scenes where the card is fully visible and found an average displacement of 0.619 pixels with a standard deviation of 0.610 pixels. Further details can be found in Appendix B.2. These verification methods demonstrate that our dataset is aligned with minimal error.

### 3.2 BVI-RLV dataset

In total, we acquired 40 scenes at two different low-light levels, including 6 scenes of moving objects with a static background (objects were placed on the dolly for repeatable motions). This resulted in 31,800 image pairs with various motion settings, where 100% indicates normal light, which can be used as a reference or ground truth. The number of frames varied based on the dolly’s speed. Each scene contains a ‘Datacolor SpyderCheckr24’ card, which can be used for camera calibration and as a white balance target. This provides a set of homogeneous patches as a reference. Full details and example scenes can be found in Appendix B.1.

We captured both static backgrounds with moving objects and fully dynamic scenes. For static backgrounds, objects were placed on a dolly while the camera remained on a tripod. For dynamic content, the camera was mounted on a dolly, creating both linear and nonlinear motions. Three camera positions and movements relative to the dolly’s direction were configured: i) *parallel* (camera axis perpendicular to dolly movement), ii) *angle* (camera axis at a 30-degree angle to dolly movement, see Fig. 3 left), and iii) *rotation* (camera rotation in yaw angle while dolly moves). Dolly speeds were either constant or varied after clipping, denoted as *linear* and *nonlinear*. Fig. 1 shows various captured motions. The x-t planes of four example videos reveal different movements. Mario3 shows linear motion of the foreground object with a static background. The dynamic scene Book1 transitions from fast motion to slow and back to fast. Mario1 exhibits nonlinear movement from left to right and back. The Flowers scene also features nonlinear movement. Fig. 4 reveals the noise present in the low-light scenes (for visualization, we applied histogram matching to 100% lighting). Extensive color correction is unnecessary since the standard color palette is included, aiding the training process. The right image group shows a magnified, cropped image of the mug in the Kitchen scene. The letters (‘A cup of’) in the low-light video appear thicker than in the normal-light one due to motion blur.

**Why not synthetic low-light videos?** While the number of datasets captured under real low-light conditions is limited, synthetic image samples have expanded research activities in this field [25]. However, it is important to note that synthetic distortions for videos are often oversimplified. As mentioned earlier, low-light conditions combine multiple distortion types. Simulating low-light videos from raw still images is not ideal due to the temporal component of noise. Motion blur and focus blur in videos also complicate blur characteristics compared to still images, so a stop-motion approach is not appropriate. As far as we know, these problems remain unsolved.

## 4 Benchmarks

We propose four benchmarking methods that can be executed on a single NVIDIA GeForce RTX 3090 GPU. The main architectural components of these methods are illustrated in Figure 5. The first model, PCDUNet, is a pure CNN architecture (see Section 5). The second model, STA-SUNet, integrates the Transformer (details in [26]). Additionally, we introduce two novel LLVE models, BVI-CDM and BVI-Mamba, which are based on conditional diffusion models [27] and state space models [28, 29], respectively.

**BVI Conditional Diffusion Model (BVI-CDM).** Inspired by DiffLL [30], designed for low-light image enhancement in the wavelet domain, we here establish the BVI-CDM model specifically for low-light videos, as shown in Fig. 5. Each frame is decomposed into the low-frequency (LF) and high-frequency (HF) subbands using 2D Haar wavelets with  $K$  decomposition levels. With reduced size, LF is enhanced by a diffusion model, thereby reducing complexity and memory usage. We use  $N$  frames as conditioning and modify the denoiser used in DiffLL by additionally performing feature alignment and fusion (FAF) in the latent space. FAF combines the Pyramid, Cascading, and Deformable (PCD) alignment and Temporal-Spatial Attention (TSA) modules used in EDVR [31]. For HF, unlike DiffLL, we propose a detailed enhancement and denoising module (DED) that suppresses noise using interscale attentions (replicating bivariate shrinkage [32]) with 3D deformable convolution, improving detail extraction and visual quality. More details are provided in Appendix C.

**BVI-Mamba.** Inspired by recent Mamba [28] and its variants for vision tasks [29, 33], featuring their linear computational complexity for long sequence modeling, we propose the BVI-Mamba for LLVE. The overall framework of BVI-Mamba is akin to STA-SUNet, but we replace all the Swin Transformer blocks [34] in the reconstruction module with the State Space Models (SSMs) with 2D Selective Scan (SS2D) module [29]. A recap of the concepts of SSM and SS2D is provided in Appendix D.

## 5 Experiments and discussion

This section examines the importance of fully registered video pairs in the development of low-light video enhancement methods. We compared our proposed dataset with existing ones by using them to train several state-of-the-art methods for low-light enhancement and video restoration, as well as our benchmarks. In all experiments using our dataset, we randomly selected 32 scenes for training and allocated the remaining scenes for testing. These were fixed for all experiments.

**Importance of dynamic video data.** This section explains why video datasets with motion are needed for video enhancement, rather than image or static video datasets as suggested by Chen et al. [1]. We argue that temporal information is crucial for minimizing inconsistencies, and motion data is essential for handling dynamic scenes. At 24 fps, flicker becomes noticeable because our perception mechanism can detect 24 Hz flicker [35]. Temporal consistency is crucial, as rapid brightness or color changes cause unpleasant viewing. To investigate, we trained models with multiple successive frames and compared them to single-frame inputs. We used UNet for single-frame input, and for multiple frames, we added PCD alignment [31], followed by UNet (referred to as PCDUNet), which is significantly lighter in weight than EDVR. Both models were trained with our dataset.

Chen et al. [1] suggest that a model trained on static videos can generalize to dynamic videos by randomly selecting two frames to train the network. However, we argue that *motion information* is crucial for effective low-light video enhancement. We tested this by modifying PCDUNet to output multiple frames and calculate loss with multiple ground truth frames, leveraging motion information for better results. This cannot be achieved with a network trained on static scenes. The results are shown in Table 2.

Table 2: Comparison of results with and without using temporal (T) and motion (M) information.

Use	Methods	PSNR	SSIM
-	SI/SO	21.78	0.770
T	MI/SO	24.48	0.844
T+M	MI/MO	25.23	0.877

S=Single, M=Multiple,  
I=Input, O=Output

**Dataset comparison.** We evaluated the training effectiveness of our datasets with various low-light video enhancement methods, including SMOID-Net [10], SDSNet [2], our PCDUNet, STA-SUNet, BVI-CDM and BVI-Mamba, as well as state-of-the-art video restoration technique, EDVR [31]. We also modified CGAN [36] to accept multiple frames as input, calling it mo-CGAN. Additionally, we investigated the performance of image-based enhancement methods for applications requiring faster and lower computation, specifically RIDNet [37] and SwinIR [34].

We compared the performances of these models trained with our datasets to those trained with existing datasets: DRV [1] (only standard RGB format with 8-bit depth is publicly available), SDSNet [2], and DID [3]. When dividing the data for training and evaluation, we followed to the parameters predefined in the original papers. The training-to-testing ratios were 73:27 for DRV, 84:16 for SDSNet and 326:87 for DID. In our dataset, we chose an intermediary approach by randomly splitting our datasets into 80% for training and 20% for testing, so 32 scenes for training listed in Appendix B.1. The training parameters were also aligned with those outlined in the original papers, ensuring consistency across all datasets for a fair comparison. If the training information was not provided in the original papers, we trained each model with 200k iterations. The results in Table 3 show the average performance across four datasets. Models trained with our dataset perform better in low-light enhancement than those trained with other datasets. The visual results presented in Fig. 6 are consistent with these objective findings.

**Benchmark performance.** We benchmark BVI-Mamba against BVI-CDM, a diffusion-based model that is the best-performing among existing architectures, using our proposed BVI-RLV dataset. BVI-Mamba demonstrates its potential to outperform BVI-CDM as indicated in Table 4, when both models are trained and tested on our dataset. To further assess their generalization when there are domain shifts, we report results on the test sets from DRV [1], SDSNet [2], and DID [3]. As shown in Table 4, BVI-Mamba achieves higher results than BVI-CDM on all tests, except for a slight decrease in PSNR on the DID test set (-0.13 dB). However, the average improvements of BVI-Mamba over BVI-CDM are 3.3%, 5.5%, and 16.7% on PSNR, SSIM and LPIPS, respectively.

**Scene variety.** Some objects were reused in different scenes in our dataset, but we varied their angles and distances from the camera, both in-focus and out-of-focus (partially similar to varying DoF). These scenes were also captured with different motions, which should mitigate the risk of overfitting due to fixed ISO and light levels, and using a specific camera. These are evident in the performance

Table 3: Performance comparison (PSNR $\uparrow$ /SSIM $\uparrow$ /LPIPS $\downarrow$ ) of the models trained with different datasets. The reported results are the average of the test sets from the four datasets. **Bold** indicates the best performance of each method. Image-based models are marked in gray.

	DRV [1]	SDSD [2]	DID [3]	BVI-RLV
	PSNR/SSIM/LPIPS	PSNR/SSIM/LPIPS	PSNR/SSIM/LPIPS	PSNR/SSIM/LPIPS
RIDNet [37]	18.43/0.678/ -	18.15/0.675/ -	<b>20.88/0.762/ -</b>	19.69/0.756/ -
SwinIR [34]	15.22/0.707/ -	11.00/0.436/ -	11.58/0.588/ -	<b>17.54/0.733/ -</b>
mo-CGAN [36]	15.84/0.456/ -	14.25/0.431/ -	15.87/0.512/ -	<b>17.41/0.557/ -</b>
EDVR [31]	15.73/0.598/ -	16.20/0.640/ -	19.53/0.701/ -	<b>20.12/0.756/ -</b>
SMOID-Net [10]	17.66/0.541/ -	14.92/0.501/ -	17.62/0.554/ -	<b>17.98/0.621/ -</b>
SDSD-Net [2]	16.31/0.587/ -	16.31/0.587/ -	<b>19.05/0.652/ -</b>	18.05/0.690/ -
PCDUNet	15.00/0.492/0.422	17.07/0.677/0.356	18.91/0.725/ <b>0.305</b>	<b>19.50/0.757/0.316</b>
STA-SUNet [26]	14.19/0.424/0.424	16.93/0.608/0.475	19.61/0.714/0.385	<b>20.64/0.765/0.243</b>
BVI-CDM	19.56/0.575/0.350	21.00/0.746/0.292	19.44/0.683/0.199	<b>22.20/0.773/0.175</b>

Table 4: Performance of the benchmarks trained with BVI-RLV dataset and tested on different datasets. **Bold** indicates the best performance of each method.

	DRV [1]	SDSD [2]	DID [3]	BVI-RLV
	PSNR/SSIM/LPIPS	PSNR/SSIM/LPIPS	PSNR/SSIM/LPIPS	PSNR/SSIM/LPIPS
BVI-CDM	18.54/0.686/0.269	21.48/0.757/0.156	<b>18.86/0.770/0.180</b>	29.93/0.897/0.097
BVI-Mamba	<b>18.80/0.720/0.238</b>	<b>22.96/0.811/0.139</b>	18.73/ <b>0.838/0.137</b>	<b>31.22/0.912/0.071</b>

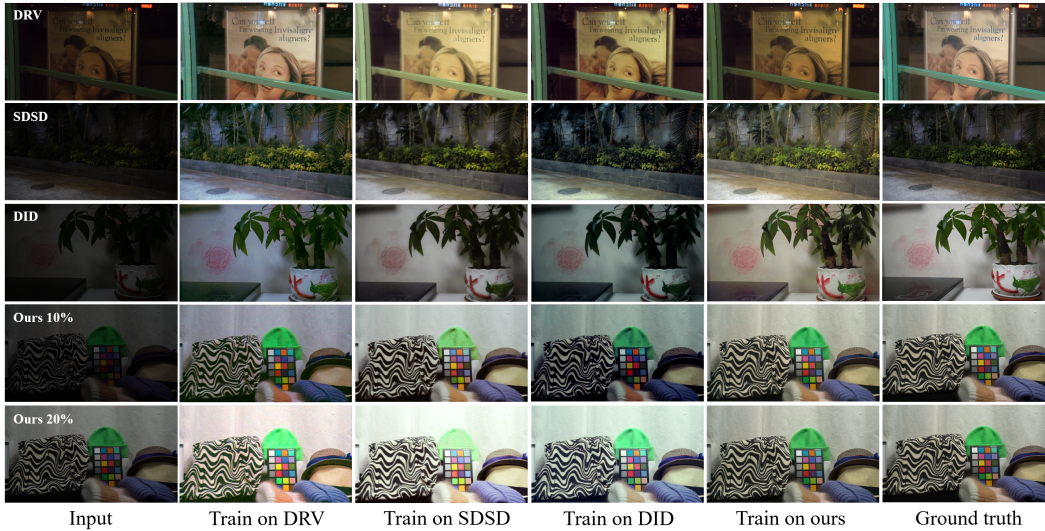


Figure 6: Subjective results of the BVI-CDM model trained on different datasets, and tested on different datasets. The test results for the DRV, SDS, and DID datasets are displayed from top to down. The two bottom rows show the test results on our datasets at light levels of 10% and 20%



Figure 7: Subjective results of the STA-SUNet model trained on different datasets, and tested on the outdoor scenes of DID.

of our dataset-trained models when tested on various datasets. Particularly noteworthy is their effectiveness in outdoor scenes, despite being captured in a controlled environment, as demonstrated in Fig. 6 (DID test video) and Fig. 7. We investigated the variety of content within the datasets (see Appendix E.5). Among the four datasets, our BVI-RLV contains stronger structures and comparable fine details to the others.

**Limitation in objective evaluation.** As brightness perception in videos can be subjective, the objective results in Table 3 may not fully capture this aspect. Hence, we investigated the scenario where the preferred brightness level is known by applying histogram matching to the reference, which was the first frame of normal-light videos, as post-processing. We found that the PSNR results for all datasets were significantly improved, as shown in Table 5, and the models trained with our BVI-RLV still produced the best results. Additional results are in the Appendix F.

**Limitation due to complexity.** In real scenarios, brightness levels are unknown and can vary widely. While preprocessing techniques like intensity normalization can be applied, most commercial cameras already capture a wide range of intensities, so min-max normalization has little effect. Adjusting the aperture or applying histogram equalization can enhance noise. Reliable datasets are essential for deep learning and for analyzing low-light signals in relation to normal-light ones. Combining existing datasets (e.g., DID and our dataset) increases training data variation but also extends the training process. Current video processing methods can take a week to converge on a single GPU, and limited memory can worsen this. Therefore, considering a lightweight model is necessary.

**Potential negative societal impact.** Low-light video enhancement technology poses risks like privacy invasion, increased surveillance, and security threats. It can be misused by criminals and may create a false sense of security and spread misinformation through manipulated footage.

## 6 Conclusion

This paper presents a new dataset designed for low-light video enhancement. The dataset includes forty dynamic scenes captured under two low-light levels, ensuring full registration in both spatial and temporal dimensions with corresponding normal-light videos serving as ground truth. This dataset facilitates the development of supervised learning models and enables full-reference quality assessment. Four deep learning methods based on different current technologies are provided and serve as baselines for evaluating improvements in future methods.

**Acknowledgments.** This work was supported by the UKRI MyWorld Strength in Places Programme (SIPF00006/1) and Bristol+Bath Creative R+D under AHRC grant (AH/S002936/1).

## References

- [1] Chen Chen, Qifeng Chen, Minh N. Do, and Vladlen Koltun. Seeing motion in the dark. In *Proceedings of the IEEE/CVF International Conference on Computer Vision (ICCV)*, October 2019.
- [2] Ruixing Wang, Xiaogang Xu, Chi-Wing Fu, Jiangbo Lu, Bei Yu, and Jiaya Jia. Seeing dynamic scene in the dark: High-quality video dataset with mechatronic alignment. In *ICCV*, 2021.
- [3] Huiyuan Fu, Wenkai Zheng, Xicong Wang, Jiakuan Wang, Heng Zhang, and Huadong Ma. Dancing in the dark: A benchmark towards general low-light video enhancement. In *Proceedings of the IEEE/CVF International Conference on Computer Vision (ICCV)*, 2023.
- [4] Valery Dewil, Jeremy Anger, Axel Davy, Thibaud Ehret, Gabriele Facciolo, and Pablo Arias. Self-supervised training for blind multi-frame video denoising. In *Proceedings of the IEEE/CVF Winter Conference on Applications of Computer Vision (WACV)*, pages 2724–2734, January 2021.
- [5] Jinxiu Liang, Yong Xu, Yuhui Quan, Boxin Shi, and Hui Ji. Self-supervised low-light image enhancement using discrepant untrained network priors. *IEEE Transactions on Circuits and Systems for Video Technology*, 32(11):7332–7345, 2022.

Table 5: PSNR after post-processing with histogram matching to reference

Trained	DRV	SDSD	DID	Ours
SwinIR	29.70	27.60	30.53	<b>31.97</b>
mo-CGAN	31.04	29.35	33.68	<b>34.66</b>
BVI-CDM	27.93	29.39	28.75	<b>29.79</b>

- [6] N. Anantrasirichai and David Bull. Contextual colorization and denoising for low-light ultra high resolution sequences. In *ICIP proc.*, pages 1614–1618, 2021.
- [7] Alexandra Malyugina, Nantheera Anantrasirichai, and David Bull. A topological loss function for image denoising on a new BVI-lowligh dataset. *Signal Processing*, 211, 2023.
- [8] Kristina Monakhova, Stephan R. Richter, Laura Waller, and Vladlen Koltun. Dancing under the stars: video denoising in starlight. In *2022 IEEE/CVF Conference on Computer Vision and Pattern Recognition (CVPR)*, pages 16220–16230, 2022.
- [9] Fisher Yu, Haofeng Chen, Xin Wang, Wenqi Xian, Yingying Chen, Fangchen Liu, Vashisht Madhavan, and Trevor Darrell. BDD100K: A diverse driving dataset for heterogeneous multitask learning. In *Proceedings of the IEEE/CVF Conference on Computer Vision and Pattern Recognition (CVPR)*, June 2020.
- [10] Haiyang Jiang and Yinqiang Zheng. Learning to see moving objects in the dark. In *2019 IEEE/CVF International Conference on Computer Vision (ICCV)*, pages 7323–7332, 2019.
- [11] Huanjing Yue, Cong Cao, Lei Liao, Ronghe Chu, and Jingyu Yang. Supervised raw video denoising with a benchmark dataset on dynamic scenes. In *2020 IEEE/CVF Conference on Computer Vision and Pattern Recognition (CVPR)*, pages 2298–2307, 2020.
- [12] Gerald Schaefer. An uncompressed benchmark image dataset for colour imaging. In *2010 IEEE International Conference on Image Processing*, pages 3537–3540, 2010.
- [13] Tobias Plötz and Stefan Roth. Benchmarking denoising algorithms with real photographs. In *2017 IEEE Conference on Computer Vision and Pattern Recognition (CVPR)*, pages 2750–2759, 2017.
- [14] A. Abdelhamed, S. Lin, and M.-S. Brown. A high-quality denoising dataset for smartphone cameras. In *CVPR proc.*, pages 1692–1700, 2018.
- [15] Chongyi Li, Chunle Guo, Linghao Han, Jun Jiang, Ming-Ming Cheng, Jinwei Gu, and Chen Change Loy. Low-light image and video enhancement using deep learning: A survey. *IEEE Transactions on Pattern Analysis and Machine Intelligence*, 44(12):9396–9416, 2022.
- [16] Olaf Ronneberger, Philipp Fischer, and Thomas Brox. U-net: Convolutional networks for biomedical image segmentation. In *Medical Image Computing and Computer-Assisted Intervention (MICCAI)*, 2015.
- [17] Kun Zhou, Wenbo Li, Liying Lu, Xiaoguang Han, and Jiangbo Lu. Revisiting temporal alignment for video restoration. In *Proceedings of the IEEE/CVF Conference on Computer Vision and Pattern Recognition*, 2022.
- [18] Wei Wang, Xin Chen, Cheng Yang, Xiang Li, Xuemei Hu, and Tao Yue. Enhancing low light videos by exploring high sensitivity camera noise. In *2019 IEEE/CVF International Conference on Computer Vision (ICCV)*, pages 4110–4118, 2019.
- [19] J. Dai, H. Qi, Y. Xiong, Y. Li, G. Zhang, H. Hu, and Y. Wei. Deformable convolutional networks. In *ICCV*, pages 764–773, Oct 2017.
- [20] Lin Liu, Junfeng An, Jianzhuang Liu, Shanxin Yuan, Xiangyu Chen, Wengang Zhou, Houqiang Li, Yan Feng Wang, and Qi Tian. Low-light video enhancement with synthetic event guidance. *Proceedings of the AAAI Conference on Artificial Intelligence*, 37(2):1692–1700, Jun. 2023.
- [21] Danai Triantafyllidou, Sean Moran, Steven McDonagh, Sarah Parisot, and Gregory Slabaugh. Low light video enhancement using synthetic data produced with an intermediate domain mapping. In *European Conference on Computer Vision*, pages 103–119. Springer, 2020.
- [22] N. Anantrasirichai, Alin Achim, and David Bull. Atmospheric turbulence mitigation for sequences with moving objects using recursive image fusion. In *2018 25th IEEE International Conference on Image Processing (ICIP)*, pages 2895–2899, 2018.
- [23] Dinggang Shen. Image registration by local histogram matching. *Pattern Recognition*, 40(4):1161–1172, 2007.
- [24] J.N. Sarvaiya, Suprava Patnaik, and Salman Bombaywala. Image registration by template matching using normalized cross-correlation. In *2009 International Conference on Advances in Computing, Control, and Telecommunication Technologies*, pages 819–822, 2009.

- [25] Abdelrahman Abdelhamed, Marcus Brubaker, and Michael Brown. Noise flow: Noise modeling with conditional normalizing flows. In *2019 IEEE/CVF International Conference on Computer Vision (ICCV)*, pages 3165–3173, 2019.
- [26] Ruirui Lin, Nantheera Anantrasirichai, Alexandra Malyugina, and David Bull. A spatio-temporal aligned sunet model for low-light video enhancement. In *Submitting to IEEE International Conference on Image Processing*, 2024.
- [27] Jiaming Song, Chenlin Meng, and Stefano Ermon. Denoising diffusion implicit models. *ICLR*, 2021.
- [28] Albert Gu and Tri Dao. Mamba: Linear-time sequence modeling with selective state spaces. *arXiv preprint arXiv:2312.00752*, 2023.
- [29] Yue Liu, Yunjie Tian, Yuzhong Zhao, Hongtian Yu, Lingxi Xie, Yaowei Wang, Qixiang Ye, and Yunfan Liu. Vmamba: Visual state space model. *arXiv preprint arXiv:2401.10166*, 2024.
- [30] Hai Jiang, Ao Luo, Haoqiang Fan, Songchen Han, and Shuaicheng Liu. Low-light image enhancement with wavelet-based diffusion models. *ACM Transactions on Graphics (TOG)*, 42(6):1–14, 2023.
- [31] Xintao Wang, Kelvin C.K. Chan, Ke Yu, Chao Dong, and Chen Change Loy. EDVR: Video restoration with enhanced deformable convolutional networks. In *The IEEE Conference on Computer Vision and Pattern Recognition (CVPR) Workshops*, June 2019.
- [32] L. Sendur and I.W. Selesnick. Bivariate shrinkage functions for wavelet-based denoising exploiting interscale dependency. *IEEE Transactions on Signal Processing*, 50(11):2744–2756, 2002.
- [33] Lianghai Zhu, Bencheng Liao, Qian Zhang, Xinlong Wang, Wenyu Liu, and Xinggang Wang. Vision mamba: Efficient visual representation learning with bidirectional state space model. *arXiv preprint arXiv:2401.09417*, 2024.
- [34] Jingyun Liang, Jie Zhang Cao, Guolei Sun, Kai Zhang, Luc Van Gool, and Radu Timofte. Swinir: Image restoration using swin transformer. In *2021 IEEE/CVF International Conference on Computer Vision Workshops (ICCVW)*, pages 1833–1844, 2021.
- [35] Alex O. Holcombe. Seeing slow and seeing fast: two limits on perception. *Trends in Cognitive Sciences*, pages 216–221, 2009.
- [36] Ting-Chun Wang, Ming-Yu Liu, Jun-Yan Zhu, Andrew Tao, Jan Kautz, and Bryan Catanzaro. High-resolution image synthesis and semantic manipulation with conditional gans. In *2018 IEEE/CVF Conference on Computer Vision and Pattern Recognition*, pages 8798–8807, 2018.
- [37] Saeed Anwar and Nick Barnes. Real image denoising with feature attention. In *2019 IEEE/CVF International Conference on Computer Vision (ICCV)*, pages 3155–3164, 2019.